Comparison of dynamic susceptibility contrast-MRI perfusion quantification methods in the presence of delay and dispersion.

Bianca Maan[a] and Rita Lopes Simões[a], Frederick J.A. Meijer[b], W. Klaas Jan Renema[b], Cornelis H. Slump[a]

[a] MIRA Institute for Biomedical Technology and Technical Medicine, Signals and Systems group, University of Twente, the Netherlands;
[b] Radboud University Hospital Nijmegen, Department of Radiology, the Netherlands

ABSTRACT

The perfusion of the brain is essential to maintain brain function. Stroke is an example of a decrease in blood flow and reduced perfusion. During ischemic stroke the blood flow to tissue is hampered due to a clot inside a vessel. To investigate the recovery of stroke patients, follow up studies are necessary. MRI is the preferred imaging modality for follow up because of the absence of radiation dose concerns, contrary to CT. Dynamic Susceptibility Contrast (DSC) MRI is an imaging technique used for measuring perfusion of the brain, however, is not standard applied in the clinical routine due to lack of immediate patient benefit. Several post processing algorithms are described in the literature to obtain cerebral blood flow (CBF). The quantification of CBF relies on the deconvolution of a tracer concentration-time curve in an arterial and a tissue voxel. There are several methods to obtain this deconvolution based on singular-value decomposition (SVD). This contribution describes a comparison between the different approaches as currently there is no best practice for (all) clinical relevant situations. We investigate the influence of tracer delay, dispersion and recirculation on the performance of the methods. In the presence of negative delays, the truncated SVD approach overestimates the CBF. Block-circulant and reformulated SVD are delay-independent. Due to its delay dependent behavior, the truncated SVD approach performs worse in the presence of dispersion as well. However all SVD approaches are dependent on the amount of dispersion. Moreover, we observe that the optimal truncation parameter varies when recirculation is added to noisy data, suggesting that, in practice, these methods are not immune to tracer recirculation. Finally, applying the methods to clinical data resulted in a large variability of the CBF estimates. Block-circulant SVD will work in all situations and is the method with the highest potential.

Keywords: Dynamic susceptibility contrast, perfusion, deconvolution, stroke, recirculation, reformulated SVD, block-circulant SVD, singular value decomposition

1. INTRODUCTION

Cerebral perfusion is defined as the delivery of blood to the tissues at the capillary level.[1] Stroke is a vascular disease characterized by a decrease in the blood flow and thus reduced perfusion in the brain. It is the second cause of death and a leading cause of long-term disability worldwide. Ischemic stroke, caused by the blockage of a vessel that supplies part of the brain, is the most common type of stroke.[2]

The imaging techniques used in the assessment of perfusion are Positron Emission Tomography (PET),[3,4] Single Photon Emission Computed Tomography (SPECT),[5] Xenon-enhanced Computed Tomography (Xe-CT),[6,7] dynamic perfusion computed tomography[8,9] and Magnetic Resonance Imaging (MRI).[10,11] The two MRI perfusion techniques available are Arterial Spin Labelling (ASL) and Dynamic Susceptibility Contrast (DSC) MRI.

All these techniques provide quantitative measures of perfusion, such as the Cerebral Blood Volume (CBV), the Cerebral Blood Flow (CBF) and the Mean Transit Time (MTT). H_2 ^{15}O PET is usually selected as gold

standard in brain perfusion imaging.[3, 4, 12] For clinical purposes, this method has substantial disadvantages, including the need for an arterial catheter to sample the arterial tracer concentration over time, the use of radioactivity and the limited availability of PET centers with a cyclotron for the required on-site production of the radionuclide.

DSC-MRI is a widely used technique. The fact that it is less invasive than PET makes it more suitable for monitoring the progression of the stroke or the effect of a therapy in follow up studies. It consists of an intravenous injection of a contrast agent (typically a gadolinium chelate, Gd-DTPA) and the subsequent monitoring of its first passage in the brain tissues via the fast acquisition of a series of T_2 or T_2^* weighted images.[13] The resulting signal-time curves can be post-processed using the perfusion model of Meier-Zierler for non-diffusible tracers in order to determine the hemodynamic parameters.[14]

First, the signal intensities of all voxels are converted to tracer concentrations. Most authors assume that the tissue concentration of the contrast agent is proportional to the change in the transversal relaxation rate.[1, 15–17] The relationship between the signal intensity, $S(t)$, and the change in relaxation rate, $\Delta R_2(t)$, during the passage of the bolus is then given by

$$S(t) = S_0 e^{-TE \cdot \Delta R_2(t)}, \tag{1}$$

where S_0 denotes the precontrast signal and TE the echo time. The concentration $C(t)$ can then be calculated using

$$C(t) = -\frac{1}{TE} \ln\left(\frac{S(t)}{S_0}\right), \tag{2}$$

where $C(t)$ is the contrast agent concentration of the voxel at time t. By detecting the arterial as well as the tissue concentration as a function of time, the cerebral blood flow (CBF) can be calculated. The arterial concentration time curve is also called the arterial input function (AIF) because this curve is the theoretical concentration-time input for all tissue voxels. In practice it is not possible to measure the true AIF for every voxel. Usually one AIF is estimated for the whole brain from a major vessel such as the middle cerebral artery by selection of one voxel or a region of interest (ROI). Therefore, the estimated AIF may undergo delay and/or dispersion between the position of AIF recording and the tissue voxels.[1] This needs to be taken into account in the determination of the perfusion parameters.

The CBF is defined as the volume of blood moving through a given brain region per unit time, representing the capillary flow in the tissue. CBF has units of milliliters of blood per 100 gram of brain tissue per minute (mL/100 g/min).[18] To calculate the CBF the residue data $R(t)$ has to be known. $R(t)$ is the fraction of the injected tracer still present in the vasculature at time t after an in theory infinitely short injection of tracer into the artery. $R(t)$ can be expressed as

$$R(t) = 1 - \int_0^t h(t)dt, \tag{3}$$

with $h(t)$ the probability density function of the capillary transit times.[1, 17] The product $CBF \cdot R(t)$ is called the tissue impulse response function, as it is the tissue concentration as a result of the infinitely short AIF. However, in fact the AIF is distributed in time. The tissue concentration-time curve becomes the convolution of the tissue impulse response function and the shape of the AIF

$$\begin{aligned} C_t(t) &= CBF \int_0^t AIF(\tau)R(t-\tau)d\tau \\ &= CBF \cdot R(t) \otimes AIF(t), \end{aligned} \tag{4}$$

where $\otimes$ denotes convolution.[1, 17]

When an appropriate AIF is selected, the CBF can be determined by deconvolution. Because $R(0) = 1$, CBF should theoretically be equal to the initial height of the tissue impulse response function. However, this is only valid in the absence of delay and dispersion. Therefore, the maximum of $R(t) \cdot CBF$ is commonly chosen as value for CBF.[15, 17, 19]

Several methods have been proposed to perform the deconvolution of the concentration-time curves. A reliable method is necessary for the correct quantification of subtle perfusion changes that can be detected in follow up scans. In this work we provide a comparison of the different quantification methods that are currently used with the aim of finding the most accurate and reliable one. We evaluate the effect of the presence of delay, dispersion and recirculation in the performance of these methods using simulated data for which the perfusion values are known. Finally, we assess the variability of the results obtained with the different methodologies in datasets from 15 Transient Ischemic Attack (TIA) patients.

This article is organized as follows: Section 2 reviews the existing deconvolution approaches; section 3 describes how the data was simulated; section 4 explains the comparisons that are made, including both the description of the methods used and the respective results. In section 5, the results obtained with clinical data are presented. Finally, a general conclusion will be drawn in section 6.

2. DECONVOLUTION APPROACHES

The available deconvolution approaches can be divided into three main categories; model-dependent, model-independent and statistical approaches. This study is about the model-independent deconvolution approaches which do not require a priori assumptions regarding the vascular structure. The deconvolution function is generally not robust, which means that an infinitesimal change in $C_{Tissue}(t)$ can cause a finite change in $R(t)$. There are Fourier and algebraic techniques to deconvolve Eq. (4) which mainly differ in the way they moderate the effects of noise in the measurements. This study is focussed on the singular value decomposition (SVD) approach which is a factorization method widely used in algebraic linear inverse problems.

2.1 Singular Value Decomposition

Assuming that tissue and arterial concentrations are measured at equidistant time points $t_1, t_2, t_3, \ldots, t_N$, the convolution theorem can be approximated by a matrix equation[1, 13, 17]

$$
\begin{aligned}
C_t(t_j) &= CBF \int_0^{t_j} AIF(\tau)R(t - \tau)d\tau \\
&\approx CBF\Delta t \sum_{i=0}^{j} AIF(t_i)R(t_j - t_i),
\end{aligned}
\tag{5}
$$

Equation (5) can also be written in matrix form as

$$
\begin{pmatrix} C_t(t_1) \\ C_t(t_2) \\ \ldots \\ C_t(t_N) \end{pmatrix} = CBF \cdot \Delta t \begin{pmatrix} AIF(t_1) & 0 & \ldots & 0 \\ AIF(t_2) & AIF(t_1) & \ldots & 0 \\ \ldots & \ldots & \ddots & \ldots \\ AIF(t_N) & AIF(t_{N-1}) & \ldots & AIF(t_1) \end{pmatrix} \cdot \begin{pmatrix} R(t_1) \\ R(t_2) \\ \ldots \\ R(t_N) \end{pmatrix},
\tag{6}
$$

which can be solved iteratively for the elements of $R(t_j)$. The AIF matrix is a lower triangular matrix and Δt represents the repetition time (TR).

The algebraic approach assumes that arterial and tissue concentrations are constant between measurements. However, in dynamic MR imaging, both concentrations are expected to show variation within the temporal resolution of the measurements. Therefore Østergaard et al.[17] have introduced a modification of the AIF matrix in Eq. (6) which assumes that AIF and R(t) both vary linearly with time. The elements of the AIF matrix become

$$AIF_{ij} = \begin{cases} \Delta t(AIF(t_{i-j-1}) + 4AIF(t_{i-j}) + AIF(t_{i-j+1}))/6 & 0 \le j \le i \\ 0 & else. \end{cases} \tag{7}$$

With the SVD approach the pseudo inverse of the AIF matrix can be calculated. Using the SVD the AIF matrix can be decomposed into three matrices

$$\mathbf{AIF} = \mathbf{U} \cdot \begin{pmatrix} w_1 & 0 & \dots & \dots & 0 \\ 0 & w_2 & \dots & \dots & 0 \\ 0 & 0 & \dots & \dots & 0 \\ \dots & \dots & \dots & \dots & \dots \\ 0 & 0 & \dots & \dots & w_N \end{pmatrix} \cdot \mathbf{V}^T = \mathbf{U} \cdot \mathbf{W} \cdot \mathbf{V}^T \tag{8}$$

where U and V are orthogonal matrices, so their inverses are equal to their transposes. The inverse of $\mathbf{AIF}$ can then be written as[20]

$$\mathbf{AIF}^{-1} = \mathbf{V} \cdot \left[diag \left(\frac{1}{w_j} \right) \right] \cdot \mathbf{U}^T. \tag{9}$$

The tissue impulse response function, $CBF \cdot R(t)$, can thus be calculated using

$$CBF \cdot R(t) = \mathbf{V} \cdot \left[diag \left(\frac{1}{w_j} \right) \right] \cdot \left(\mathbf{U}^T C(t) \right). \tag{10}$$

The smallest singular values in matrix $\mathbf{W}$ correspond to high frequencies. In an actual calculation of the SVD, even singular values that theoretically should be zero will show up as extremely small but non-zero values in the matrix $\mathbf{W}$. This is caused by round-off errors and noise in the data. A direct application of the calculated matrix $\mathbf{W}$ will produce large oscillations in the final solution. Regularization refers to mathematical methods which improve the stability in such problems.

Truncated SVD (tSVD) is a straightforward regularization method which treats all singular values below a certain threshold (P_{SVD}) as exact zeros. Using this method the effects of noise are reduced. However, a high threshold can lead to underestimation of the CBF.[21]

2.1.1 Alternative SVD approaches

The standard SVD approach is delay sensitive. Nowadays there are new, slightly modified, SVD approaches such as reformulated SVD[22] (rSVD) and block-circulant SVD[15] (bcSVD) which are reported to be delay insensitive.

With rSVD the first nonzero estimate of the residue function is obtained at time $t = T_{OFFSET}$. The parameter T_{OFFSET} must represent a time larger than the absolute value of the largest expected experimental negative arrival time plus the duration of signal distortions introduced when discarding singular values. With discrete $C_t(t)$ data, this method is computationally equal to shifting the experimental $C_t(t)$ values by n samples corresponding to T_{OFFSET}. After this computational time shift the SVD approach is equal to the previously described SVD approach.[22]

With bcSVD both the AIF matrix and the $C_t(t)$ vector are changed. By zero-padding the N-points AIF-time and the tissue concentration-time curves to length L, where L $\ge$ 2N, time aliasing can be avoided. Secondly, the AIF matrix is changed to

$$AIF_{ij}^{\#} = \begin{cases} AIF_{i,j} & 0 \le j \le i \\ AIF_{L+i,j,0} & else. \end{cases} \tag{11}$$

Using this AIF matrix and the zero-padded tissue concentration curve with length L, the standard SVD approach can be followed.[15]

3. DATA SIMULATION

The different postprocessing methods can be compared using simulated data with known perfusion values. During the simulations first the AIF is simulated and subsequently the tissue concentration curves can be calculated.

3.1 Simulated Arterial Input Function

The AIF is simulated using a gamma-variate function with a shape and size that is obtained using a standard bolus injection scheme.[17] The analytical expression of the AIF is

$$AIF(t) = \begin{cases} 0 & t \leq t_0 \\ A\,(t - t_0)^a \cdot e^{-(t-t_0)/b} & t > t_0 \end{cases} \tag{12}$$

with A a scaling factor, t_0 the contrast arrival time and a and b are shape parameters which depend on the vasculature and blood flow. Parameters used in this study where $A = 1$, $t_0 = 20$ s, $a = 3.0$ and $b = 1.5$ s. Subsequently the recirculation is calculated by convolving the obtained AIF, with an additional delay of 8 seconds, with an exponential with a time constant of 30 seconds. All datasets are simulated with a TR of 1 second and over a time range of 250 seconds to avoid truncation of the curves.

3.2 Simulated Tissue Concentration Curve

To investigate the performance of the different deconvolution methods, tissue curves produced with an exponential residue functions $R\,(t)$ are used. The exponential residue function describes the vasculature as one single, well-mixed compartment and is given by

$$R\,(t) = \begin{cases} 0 & t < 0 \\ e^{-\frac{t}{MTT}} & 0 \leq t. \end{cases} \tag{13}$$

The MTT is the mean transit time which is the mean time for blood to perfuse a volume of tissue.

The tissue concentration curves are calculated using Eq. (4) with different values for CBF, CBV and MTT. Subsequently, the obtained concentration-time curves are converted to signal intensity-time curves using

$$S(t) = S_0 e^{-k \cdot C(t) \cdot TE} \tag{14}$$

which is equivalent to Eq. (1) including a proportionality factor k which is used to match a typical peak drop in signal intensity. For all simulations, a proportionality factor k is selected that resulted in a 40% peak signal drop at a flow rate of 60ml/100g/min and CBV = 4%. These values correspond to values typically found in human gray matter.[15] Furthermore S_0 depends on scanner hardware and software and is entirely arbitrary. During the simulations $S_0 = 100$ and TE = 30 ms are used. The signal intensity-time curve for the AIF is similarly modeled as $S(t)$, except that AIF is substituted for $C(t)$. The proportionality constant, k, is in this case selected to generate a peak signal drop of 60% as done by Wu et al.[15] To determine absolute flow values at the end of the calculations, the calculated CBF values are rescaled by the k-factors used.

3.3 Add Delay and Dispersion

To simulate delay and dispersion, the model described by Calamante et al.[23] is used. Simulation of dispersion is equivalent to a convolution of the estimated AIF with an effective residue function, $R^{(eff)} = h^*\,(t) \otimes R$, with $h^*\,(t)$ a vascular transport function[23]

$$h^*(t) = \beta \cdot e^{-\beta t} \tag{15}$$

as a first approximation for the vascular transport function. With this approximation the assumption as a well-mixed compartment is used for the vasculature. $1/\beta$ corresponds to the effective MTT of the distance between AIF recording and the tissue.

Using this model for $h^*(t)$, the effective residue function can be written as

$$R^{(eff)}(t) = \frac{\beta}{\left(\frac{1}{MTT} - \beta\right)} \cdot \left(e^{-\beta t} - e^{-t/MTT}\right). \tag{16}$$

This effective residue function is used instead of the previously described residue function to simulate dispersion. Subsequently delay of the curve can be simulated by shifting the obtained tissue curve with a time delay, t_d.

3.4 Add Noise

The obtained signal intensity-time curves are expanded into 1024 copies. Zero-mean random Gaussian noise is added to each curve to generate 1024 different curves with signal to noise ratios (SNR) of 20 and 100. The SNR is determined at the baseline of the signal curve.

3.5 Optimal P_{SVD} Calculation

Comparisons between the deconvolution methods are performed using the optimal truncation parameter, P_{SVD}. The optimal P_{SVD} is calculated using the method described by Wu et al.[15] For P_{SVD} values between 0.1% and 90%, the error at each of the 1024 iterations is calculated as

$$E_t = \frac{1}{N_f} \cdot \sum_1^{N_f} |F - F'|, \qquad (17)$$

where F is the true CBF value, F' the estimated CBF value and N_f the number of simulated CBF values. The optimal P_{SVD} is determined as the value that minimized the averaged error simultaneously over all CBV values and all 1024 iterations assuming zero time delay and no dispersion.

4. COMPARISONS

4.1 Recirculation

Kosior et al.[19] reported that CBF calculations are immune for tracer recirculation using noise-free concentration curves. In practice all MRI signals contain noise, therefore it is important to investigate whether CBF calculations are immune for tracer recirculation in the presence of noise as well.

4.1.1 Methods

The CBV of the simulated data is either 4% or 2%. For CBV 4% the CBF is varied between 10-70 mL/100 g/min in 10 mL/100 g/min increments. For CBV 2% CBF values are evaluated from 5-35 mL/100 g/min using 5 mL/100 g/min increments in order to maintain the same range of MTT values. To validate the findings by Kosior et al.[19] first the $CBF_{firstpass}/CBF_{recirculation}$ is calculated for noise-free curves using a non-weighted AIF matrix and a P_{SVD} of $5e^{-7}$. Subsequently noise is added to the curves and the optimal P_{SVD} values are determined for tSVD and bcSVD using the method described in subsection 3.5.

4.1.2 Results

The $CBF_{firstpass}/CBF_{recirculation}$ ratio calculated with all deconvolution approaches with noise-free curves is one. This means that the CBF estimates are not influenced by tracer recirculation. For curves including noise truncation of the eigenvalues is necessary. In Fig. 1 the mean error curves for determination of the optimal P_{SVD}'s using tSVD and curves with SNR 20 are depicted. The optimal P_{SVD} is represented by the minimum of the error curve. The optimal P_{SVD} for curves with recirculation (solid-line) is lower compared to the optimal P_{SVD} for curves without recirculation (dashed-line). However, the mean error and standard deviation of both types of curves is comparable. The obtained P_{SVD}'s are listed in Table 1.

Table 1. Optimal P_{SVD}'s for curves with and without recirculation using tSVD and bcSVD.

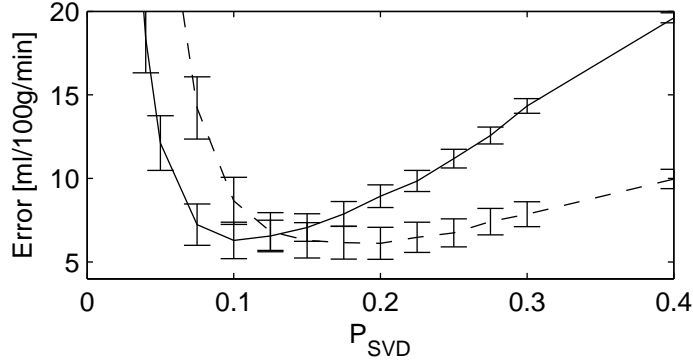|	SNR	with recirculation	without recirculation
tSVD	20	10%	20%
	100	4%	10%
bcSVD	20	7.5%	10%
	100	2%	3%

Figure 1. Mean error curve of curves with (solid-line) and without (dashed-line) recirculation using tSVD. The depicted graph is for SNR 20. The errorbars represent 1SD.

4.1.3 Discussion

Kosior et al.[19] have shown that tracer recirculation does not impact estimations of CBF using noise-free tissue concentration curves. These findings are validated for both tSVD and bcSVD. Although CBF estimates are theoretically not influenced by the presence of tracer recirculation. Figure 1 shows that there is a difference in optimal P_{SVD} for curves with and without recirculation when noise is added to the curves. Using one fixed P_{SVD} for a dataset containing curves both with and without recirculation, the estimation error will differ between the voxels. However, if it would be possible to determine an optimal P_{SVD} for each voxel seperately, the error and the standard deviation of the error are still equal because these are based on curves with the same SNR.

4.2 Delay and Dispersion

The AIF is usually selected in a major vessel. Therefore delay and dispersion can occur between the location of AIF measurement and the tissue.

4.2.1 Methods

To investigate the deconvolution approaches in the presence of delay or dispersion three tissue concentration-time curves are obtained with the perfusion values listed in Table 2. These curves represent gray and white matter and hypoperfused tissue.[24]

Table 2. CBV, CBF and MTT values of the three different tissue types.

Tissue	CBV (ml/100g)	CBF (ml/100g/min)	MTT (s)
Gray matter	4	60	4
White matter	2	20	6
Hypoperfused tissue	1.8	12	9

The optimal P_{SVD} is dependent on the CBF value, therefore the optimal value is calculated using the described concentration curves including curves with CBF - 10% and CBF+10%. In summary, three CBF values combined with three CBV values give nine concentration time curves involved in the optimal P_{SVD} calculation. The calculated optimal P_{SVD}'s are used for the subsequent comparisons. The P_{SVD} determined using tSVD is used for rSVD as well.

To evaluate the sensitivity of CBF estimates to differences in tracer arrival times, i.e. delay, the tissue curves are shifted with respect to the AIF from -4 till +6 seconds with increments of one second. To evaluate the sensitivity to dispersion, data is simulated with values of $1/\beta$ up to 5.5 seconds. First the analysis is done using noise-free curves and subsequently using curves with a SNR of 20 and 100.

4.2.2 Results

The optimal P_{SVD}'s for SNR 20 and 100, for both tSVD and bcSVD are listed in Table 3. These values are used during the following steps of this investigation. This comparison can be divided into two parts, namely CBF estimates calculated in the presence of delay and CBF estimates in the presence of dispersion. First the results related to delay are described.

Table 3. Optimal P_{SVD} values using tSVD and bcSVD for curves with the perfusion values listed in Tab. 2 including CBF-10% and CBF+10% curves.

SNR	tSVD	bcSVD
20	10%	7.5%
100	5%	2%

Figure 2 shows the $CBF_{estimated}/CBF_{true}$ ratio for noise-free curves calculated using tSVD and bcSVD. rSVD shows exactly the same results as bcSVD, for clarity only bcSVD is shown. CBF estimates calculated with the tSVD approach are overestimated in the presence of negative delays and well estimated with delays greater than zero. Furthermore the figure shows that CBF estimates calculated with bcSVD and rSVD are delay independent within this range of delays.
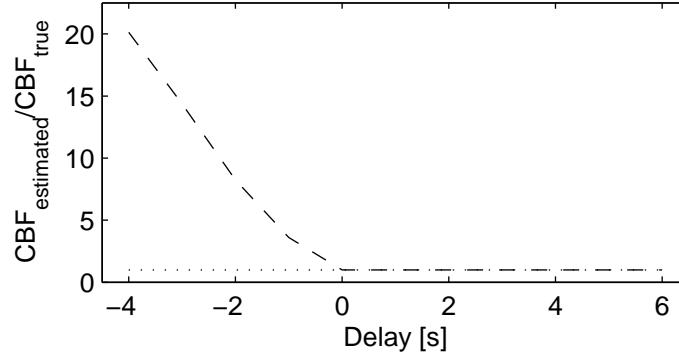

Figure 2. The effect of delay on CBF estimates of noise-free hypoperfused tissue curves. The plot shows the ratio between the CBF estimates and the true CBF. The graph includes tSVD (dashed-line) and block-circulant SVD (dotted-line).

In the presence of noise the same patterns can be recognized. Figure 3 shows the $CBF_{estimated}/CBF_{true}$ ratio for CBV 4% and SNR 100. It is found that regardless of the CBV and CBF values tSVD overestimates CBF for negative delays and performs equal to bcSVD and rSVD for delays greater than one second.

The $CBF_{estimated}/CBF_{nodispersion}$ ratio (solid-line) for noise-free concentration curves in Fig. 4 shows that all deconvolution approaches perform equal and are dependent on the amount of dispersion. When noise is added to the curves dependency on dispersion is seen as well. The figure shows that the delay independent approaches provide a higher $CBF_{estimated}/CBF_{nodispersion}$ ratio compared to delay dependent approaches.

4.2.3 Discussion

The $CBF_{estimated}/CBF_{true}$ ratio shows that the CBF estimates calculated with the tSVD approach are dependent of the delay. In the presence of negative delays, i.e. the peak of the tissue concentration curve will appear before the peak in the AIF, the tSVD approach will overestimate the CBF values. For delays equal to or larger than zero seconds tSVD becomes delay independent. bcSVD and rSVD approaches are delay independent for negative delays as well. Also when noise is added to the curves, bcSVD and rSVD are able to estimate CBF near the true CBF for negative delays. With noise the tSVD approach is delay independent for delays larger than one second.

The bcSVD and rSVD approaches seem to be delay independent. However, the delay is varied from -4 till 6 seconds with increments of 1 second, which is equal to the TR of the signal. Salluzzi et al.[25] reported that the $CBF_{estimated}/CBF_{true}$ changes with a period equal to TR. This variation is unwanted. When different
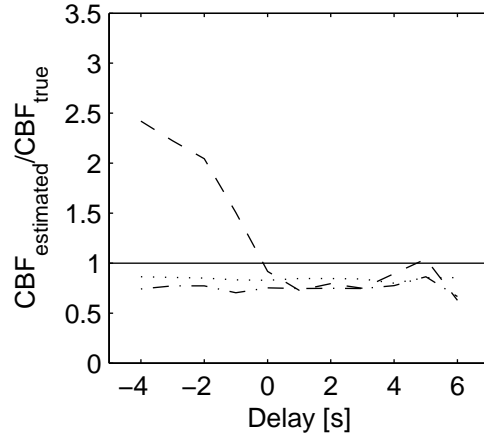
Figure 3. The effect of delay on CBF estimates. The plot shows the ratio between the CBF estimates and the true CBF for a curve representing gray matter with a SNR of 100. The tSVD (dashed-line), rSVD (dash-dot-line) and block-circulant SVD (dotted-line) are shown together with the ideal ratio (solid-line).
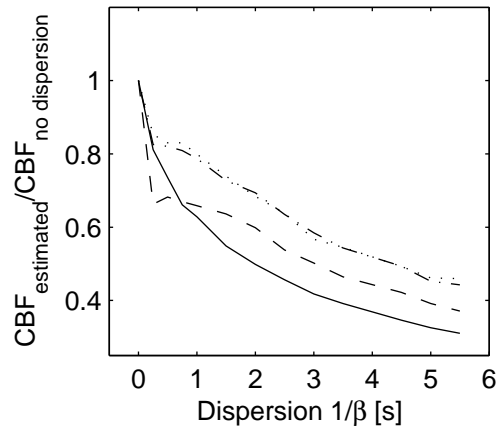

Figure 4. The effect of dispersion on CBF estimates. The plot shows the ratio between the CBF estimates and CBF estimate of a curve without dispersion representing gray matter with a SNR of 100. The solid line shows the CBF estimates calculated with noise-free curves. tSVD (dashed-line), rSVD (dash-dot-line) and bcSVD (dotted-line) are the approaches used.

voxels have different delays, the error of the CBF estimates will differ between the voxels as well. So further investigation to the delay independency of block-circulant and rSVD is necessary.

When dispersion is added to the noise-free tissue concentration curves, all approaches are unable to reproduce the true CBF. This is reported in several other articles as well.[23, 26, 27] The performance of all methods using noise-free curves is equal. However, when noise was added to the curves, the delay independent methods perform better.

Adding dispersion to the tissue concentration curves causes broadening of the bolus and subsequently a shift of the peak. According to Ko et al.[26] this is the reason why tSVD underestimates the CBF more in the presence of bolus dispersion. This is found in our investigation as well, namely with zero seconds delay, the tSVD approach gives a higher CBF estimation compared to one second delay (see Fig. 3). Therefore the CBF estimate without dispersion and thus zero delay is higher for tSVD compared to bcSVD and rSVD. For a dispersion constant $1/\beta = 0.25$ seconds a delay of one second exists which causes a change in CBF estimate due to both the bolus broadening and the additional delay. After one second delay, comparable to $1/\beta = 0.25$ s, the $CBF_{estimated}/CBF_{true}$ ratio based on the delay becomes constant and the CBF estimates are only dependent on the amount of dispersion. Therefore the shape of the curves become equal after $1/\beta = 0.25$ s.

5. CLINICAL DATA

The analysis of the clinical data is performed retrospectively. All data is obtained between May 2006 and May 2008. The data of 15 patients, 10 female and 5 male, (age: 55.7 ± 11.4 (mean $\pm$ SD)) suffering from a TIA is used. Contrast-enhanced T2* weighted images were collected using a gradient-echo sequence (TR/TE = 2280ms/47ms) on a clinical MR scanner (Siemens Medical Solutions, Avanto, 1.5T). During the imaging sequence, a contrast agent bolus (Dotarem) was injected. All studies consisted of 19 slices with a thickness of 5 mm collected over 30 timepoints.

When clinical data is used, the true perfusion values are unknown. Therefore the CBF valus estimated using the different methods are compared in order to evaluate their variability.

5.1 Methods

From the clinical MR data, first the skull is removed from the dataset by thresholding of the image. In this investigation an automatic AIF-identification algorithm is used as described by Caroll et al.[28] All data are quantified by tSVD, rSVD and bcSVD approaches with the P_{SVD} set to 22.5% for tSVD and rSVD and 15% for bcSVD. These P_{SVD}'s are based on simulated data with an SNR of 20, which is comparable to the SNR of clinical data.[15, 29]

After calculation of the CBF maps, the percentage difference between the CBF values given by the methods is calculated. This is the difference between the two CBF estimates divided by their average value, which can be described in equation form by

$$\%Difference = \frac{M_1 - M_2}{(M_1 + M_2)/2} \cdot 100, \tag{18}$$

where M_1 and M_2 are the CBF values of method 1 and method 2 respectively. Finally the mean percentage difference and its standard deviation over all voxels in the dataset is calculated.

5.2 Results

Figure 5 shows one example of a percentage difference image for one brainslice. The figure shows that the percentage difference is not uniform over the whole brain slice. For example in the figure, the percentage difference in the white matter is negative, while the percentage difference in gray matter is positive. The mean percentage difference and the mean of the standard deviation calculated over 15 patients was 26.9 ± 26.8 for tSVD vs. rSVD, -7.25 $\pm$ 16.0 for tSVD vs. bcSVD and -33.8 $\pm$ 25.7 for rSVD vs. bcSVD.
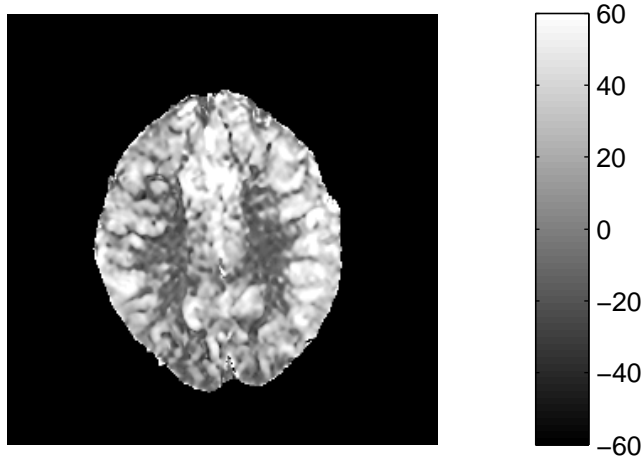
Figure 5. Percentage difference between tSVD and rSVD. A negative percentage means that tSVD provides a higher CBF estimate than rSVD. The figure shows that the percentage difference is not equal for all voxels in the brainslice. This is brain slice 13 of patient 6.

5.3 Discussion

The percentage difference is calculated over the whole acquired dataset. In some datasets, voxels of the skull are still included in the calculations because they had the same signal intensity as brain voxels. The large standard deviation shows that the percentage difference is not equal for all voxels, i.e. there is a large variability of the results.

The percentage difference seems to be related to the tissue type. To investigate the differences between the tissue types, ROIs should be drawn in the image and compared with each other. Then information about the CBF estimates between the different methods is obtained.

Finally, none of the datasets show regions of low perfusion. This was to be expected, because the datasets are from patients with a transient ischemic attack (TIA) instead of a stroke.

6. CONCLUSION

In Section 4.1 it is shown that the CBF estimates are immune for tracer recirculation using noise-free curves. However when noise is added to the curves, a difference in the optimal P_{SVD} is observed. This optimal P_{SVD} shifts cause differences in estimation errors between voxels.

tSVD is shown to be a delay dependent SVD approach, while rSVD and bcSVD are both delay independent. Furthermore it is shown that all approaches are dependent on the amount of dispersion. However, delay independent methods are preferable because of the small amount of delay which occurs during dispersion. The rSVD needs a manual input, namely the maximum amount of timeshift, and bcSVD does not use any manual input. Therefore the bcSVD method will work in all situations and is the method with the highest potential for use in the evaluation of follow up studies.

Using clinical data, a large variability of results can be observed when the different methods are applied. This suggests that further validation studies need to be carried out in order to find the best algorithm that is sensitive to detect the small changes in the patient's perfusion in the recovery process after ischemic stroke as (to be) revealed in follow up MRI scans.

REFERENCES

[1] Knutsson, L., Ståhlberg, F., and Wirestam, R., "Absolute quantification of perfusion using dynamic susceptibility contrast MRI: pitfalls and possibilities.," *MAGMA* **23**, 1–21 (Feb 2010).

[2] Donnan, G., Fisher, M., Macleod, M., and Davis, S., "Stroke," *Lancet* **371**, 1612–1623 (2008).

[3] Zaro-Weber, O., Moeller-Hartmann, W., Heiss, W., and Sobesky, J., "The performance of MRI-based cerebral blood flow measurements in acute and subacute stroke compared with 15O-water positron emission tomography: identification of penumbral flow.," *Stroke* **40**, 2413–2421 (Jul 2009).

[4] Takasawa, M., Jones, P. S., Guadagno, J. V., Christensen, S., Fryer, T. D., Harding, S., Gillard, J. H., Williams, G. B., Aigbirhio, F. I., Warburton, E. A., Østergaard, L., and Baron, J., "How reliable is perfusion MR in acute stroke? Validation and determination of the penumbra threshold against quantitative PET.," *Stroke* **39**, 870–877 (Mar 2008).

[5] Warwick, J., "Imaging of brain function using SPECT.," *Metab Brain Dis* **19**, 113–123 (Jun 2004).

[6] Rubin, G., Firlik, A. D., Levy, E. I., Pindzola, R. R., and Yonas, H., "Xenon-enhanced computed tomography cerebral blood flow measurements in acute cerebral ischemia: Review of 56 cases.," *J Stroke Cerebrovasc Dis* **8**(6), 404–411 (1999).

[7] Bews, J., Lawrence, K. S., Dunscombe, P., McClarty, B., and Kroeker, M., "A simplified method for measuring cerebral blood flow with Xenon-enhanced computed tomography.," *Clin Phys Physiol Meas* **12**, 279–287 (Aug 1991).

[8] Mayer, T. E., Hamann, G. F., Baranczyk, J., Rosengarten, B., Klotz, E., Wiesmann, M., Missler, U., Schulte-Altedorneburg, G., and Brueckmann, H. J., "Dynamic CT perfusion imaging of acute stroke.," *AJNR Am J Neuroradiol* **21**, 1441–1449 (Sep 2000).

[9] Eastwood, J. D., Lev, M. H., and Provenzale, J. M., "Perfusion CT with iodinated contrast material.," *AJR Am J Roentgenol* **180**, 3–12 (Jan 2003).

[10] van Laar, P. J., van der Grond, J., Mali, W. P. T. M., and Hendrikse, J., "Magnetic resonance evaluation of the cerebral circulation in obstructive arterial disease.," *Cerebrovasc Dis* **21**(5-6), 297–306 (2006).

[11] Sanak, D., Horak, D., Herzig, R., Hlustik, P., and Kanovsky, P., "The role of magnetic resonance imaging for acute ischemic stroke.," *Biomed Pap Med Fac Univ Palacky Olomouc Czech Repub* **153**, 181–187 (Sep 2009).

[12] Carroll, T. J., Teneggi, V., Jobin, M., Squassante, L., Treyer, V., Hany, T. F., Burger, C., Wang, L., Bye, A., Schulthess, G. K. V., and Buck, A., "Absolute quantification of cerebral blood flow with magnetic resonance, reproducibility of the method, and comparison with H2(15)O positron emission tomography.," *J Cereb Blood Flow Metab* **22**, 1149–1156 (Sep 2002).

[13] Østergaard, L., "Principles of cerebral perfusion imaging by bolus tracking.," *J Magn Reson Imaging* **22**, 710–717 (Dec 2005).

[14] Zierler, K. L., "Theoretical Basis of Indicator-Dilution Methods For Measuring Flow and Volume," *Circ Res* **10**, 393–407 (Mar. 1962).

[15] Wu, O., L. Østergaard, L., Weisskoff, R., Benner, T., Rosen, B., and Sorensen, A., "Tracer arrival timing-insensitive technique for estimating flow in MR perfusion-weighted imaging using singular value decomposition with a block-circulant deconvolution matrix," *Magn. Reson. Med.* **50**(1), 164–174 (2003).

[16] Knutsson, L., Ståhlberg, F., and Wirestam, R., "Aspects on the accuracy of cerebral perfusion parameters obtained by dynamic susceptibility contrast MRI: a simulation study.," *Magn Reson Imaging* **22**, 789–798 (Jul 2004).

[17] Østergaard, L., Weisskoff, R. M., Chesler, D. A., Gyldensted, C., and Rosen, B. R., "High resolution measurement of cerebral blood flow using intravascular tracer bolus passages. Part I: Mathematical approach and statistical analysis.," *Magn Reson Med* **36**, 715–725 (Nov 1996).

[18] Aksoy, F. G. and Lev, M. H., "Dynamic contrast-enhanced brain perfusion imaging: Technique and clinical applications," *Seminars in Ultrasound, CT, and MRI* **21**(6), 462 – 477 (2000). Advanced MR Imaging Techniques.

[19] Kosior, J. C. and Frayne, R., "Perfusion parameters derived from bolus-tracking perfusion imaging are immune to tracer recirculation.," *J Magn Reson Imaging* **31**, 753–756 (Mar 2010).

[20] Press, W., Teukolsky, S., Vetterling, W., and Flannery, B., [*Numerical recipes in C*], Cambridge University Press, 2nd edn. ed. (1992).

[21] Murase, K., Shinohara, M., and Yamazaki, Y., "Accuracy of deconvolution analysis based on singular value decomposition for quantification of cerebral blood flow using dynamic susceptibility contrast-enhanced magnetic resonance imaging.," *Phys Med Biol* **46**, 3147–3159 (Dec 2001).

[22] Smith, M., Lu, H., Trochet, S., and Frayne, R., "Removing the effect of SVD algorithmic artifacts present in quantitative MR perfusion studies," *Magn. Reson. Med.* **51**(3), 631–634 (2004).

[23] Calamante, F., Gadian, D. G., and Connelly, A., "Delay and dispersion effects in dynamic susceptibility contrast MRI: simulations using singular value decomposition.," *Magn Reson Med* **44**, 466–473 (Sep 2000).

[24] Perkiö, J., Aronen, H. J., Kangasmki, A., Liu, Y., Karonen, J., Savolainen, A., and Østergaard, L., "Evaluation of four postprocessing methods for determination of cerebral blood volume and mean transit time by dynamic susceptibility contrast imaging.," *Magn Reson Med* **47**, 973–981 (May 2002).

[25] Salluzzi, M., Frayne, R., and Smith, M., "An alternative viewpoint of the similarities and differences of SVD and FT deconvolution algorithms used for quantitative MKR perfusion studies," *Magn Reson Imaging* **23**, 481–492 (2005).

[26] Ko, L., Salluzzi, M., Frayne, R., and Smith, M., "Reexamining the quantification of perfusion MRI data in the presence of bolus dispersion.," *J Magn Reson Imaging* **25**, 639–643 (Mar 2007).

[27] Calamante, F., "Bolus dispersion issues related to the quantification of perfusion MRI Data," *Journal of magnetic resonance imaging* **22**, 718–722 (2005).

[28] Carroll, T. J., Rowley, H. A., and Haughton, V. M., "Automatic calculation of the arterial input function for cerebral perfusion imaging with MR imaging.," *Radiology* **227**, 593–600 (May 2003).

[29] Calamante, F., Gadian, D. G., and Connelly, A., "Quantification of bolus-tracking MRI: Improved characterization of the tissue residue function using Tikhonov regularization," *Magn. Reson. Med.* **50**(6), 1237–1247 (2003).